NEURAL REPETITIVE FIRING

MODIFICATIONS OF THE HODGKIN-HUXLEY AXON SUGGESTED BY EXPERIMENTAL RESULTS FROM CRUSTACEAN AXONS

JOHN A. CONNOR, DAVID WALTER, *and* RUSSELL MCKOWN,
Department of Physiology and Biophysics, University of Illinois, Urbana, Illinois 61801

ABSTRACT The Hodgkin-Huxley equations for space-clamped squid axon (18°C) have been modified to approximate voltage clamp data from repetitive-firing crustacean walking leg axons and activity in response to constant current stimulation has been computed. The m_∞ and h_∞ parameters of the sodium conductance system were shifted along the voltage axis in opposite directions so that their relative overlap was increased approximately 7 mV. Time constants, τ_m and τ_h, were moved in a similar manner. Voltage-dependent parameters of delayed potassium conductance, n_∞ and τ_n, were shifted 4.3 mV in the positive direction and τ_n was uniformly increased by a factor of 2. Leakage conductance and capacitance were unchanged. Repetitive activity of this modified circuit was qualitatively similar to that of the standard model. A fifth branch was added to the circuit representing a transient potassium conductance system present in the repetitive walking leg axons and in other repetitive neurons. This model, with various parameter choices, fired repetitively down to approximately 2 spikes/s and up to 350/s. The frequency vs. stimulus current plot could be fit well by a straight line over a decade of the low frequency range and the general appearance of the spike trains was similar to that of other repetitive neurons. Stimulus intensities were of the same order as those which produce repetitive activity in the standard Hodgkin-Huxley axon. The repetitive firing rate and first spike latency (utilization time) were found to be most strongly influenced by the inactivation time constant of the transient potassium conductance (τ_B), the delayed potassium conductance (τ_n), and the value of leakage conductance (g_L). The model presents a mechanism by which stable low frequency discharge can be generated by millisecond-order membrane conductance changes.

INTRODUCTION

This study has been undertaken to explore repetitive firing behavior of the Hodgkin-Huxley equations (22) given certain modifications to conform to voltage-clamp data from repetitive walking leg axons of crustaceans. Of primary interest has been the problem of generating stable, low-frequency discharge down to a range of 1 or 2 spikes/s (4) by means of a system of equations having parameters that vary on a millisecond or submillisecond time scale.

Dr. Walter's present address is: Control Data Corporation, Bloomington, Minn. 55431

Most neurons show a strong tendency to fire repetitively when given a constant stimulting current and many different types are capable of a large gradation of firing frequency as this stimulus is varied. The relation between frequency and stimulus is linear over a sizable frequency range for receptor-encoder neurons and the low frequency range may extend down to 1 or 2 spikes/s. A number of examples have been summarized by Fuortes and Mantegazzini (17) and Jack et al. (26). Relating this type of behavior to observable membrane conductance changes is an unresolved problem. The Hodgkin-Huxley equations, the most widely accepted quantitative formulation of membrane conductance parameters, predict repetitive activity of a rather high minimum rate (>100 spikes/s), which is rather insensitive to gradations in suprathreshold stimulus (1, 14, 25, 32). There have been several modifications of the equations to give low-frequency firing with the proper type of stimulus-frequency dependence. For example, Shapiro and Lenherr (31) increased the characteristic time constant of the potassium conductance (τ_n) in the subthreshold range and generated slower repetitive firing and improved linearity. This model may well be a good description of spinal motoneurons that appear to generate slow firing by means of a prolonged after-hyperpolarization. A second approach to modeling motoneuron-type firing was made by Kernell and Sjöholm (27). These investigators added very slow potassium conductance to the Frankenhaeuser-Huxley (15) equations for the node of Ranvier. The standard node equations generate repetitive firing activity very similar to that of the Hodgkin-Huxley equations (cf 3). The added potassium conductance produced both the after-hyperpolarization characteristics of motoneurons, low frequency discharge ($\sim$10 spikes/s), and a degree of accommodation. Dodge (13), undertaking to model conditions observed in *Carcinus* axons, shifted the potassium conductance system rate constants positive by 8 mV and reduced leakage conductance. These operations produced a very high membrane resistance in the threshold range as reported for *Carcinus* by Hodgkin (see 13) and extended the low frequency response to a point somewhat under 10 spikes/s. Frequency in the lower range, however, became an extremely sensitive function of stimulus intensity. Connor and Stevens (9) published a study of molluscan nerve somata in which repetitive activity was simulated from voltage clamp data. Simulation of repetitive activity successfully reproduced both the low-frequency firing observed in these cells and a linear frequency-stimulus relationship. The essential feature was the addition of a transient potassium conductance to other membrane parameters qualitatively similar to those of squid axon. The analysis left at least two important questions unsettled. The first was the ubiquitousness of the transient conductance in other repetitive neurons of the transducer-encoder type. The second followed as a result of the time-course of conductance changes in molluscan neurons, typically an order of magnitude greater than that observed in squid or vertebrate neurons: *i.e.*, could appropriately fast conductance changes still generate intervals of hundreds of milliseconds?

As was shown in a previous article (6), there are significant differences in the potassium conductance system or systems of repetitive crustacean axons on the one hand and of squid axon, amphibian node of Ranvier, and the nonrepetitive crustacean axons

on the other hand. The experimental part of this study will also show differences in the sodium conductance system of these two groups of cells, although not so pronounced as in the potassium system.

The strategy of this study has been to make justifiable changes in an existing system, the Hodgkin-Huxley equations, rather than pursue a complete analysis of the crustacean preparation and do a simulation for that specific data, as was done in a previous study on *Anisodoris* central neurons (9). We have chosen this formal and, we hope, more general approach for the following three reasons. First, we are unable at this time to justify a novel and adequate kinetic description of current carried by potassium ion in the repetitive-firing preparation and hence have tried to remain as close as possible to an existing scheme. Second, despite specific shortcomings of the Hodgkin-Huxley equations in fitting all of the available voltage-clamp data from axons (*c.f.* 5, 18, 24), they remain the commonly used formulation in which to cast voltage-clamp data and form the basis of the standard conceptual framework for interpreting complex electrical events in excitable cells. Third, the considerable literature on the repetitive characteristics of the equations should serve as a useful basis for criticism of this or any other analysis of repetitive activity in excitable membranes. A preliminary report has been given (10).

MATERIALS AND METHODS

Voltage clamp experiments were carried out in the double sucrose gap apparatus described in a preceding article (6). In addition to studies on *Callinectes sapidus* axons (6), more recent experiments have been performed on larger axons from *Cancer magister* to investigate details of the sodium conductance system. Feedback compensation for series resistance (23) was employed in the studies on *Cancer*. Measurements on potassium conductance systems were made at 18°C, on the sodium conductance at 8°C. Physiological saline followed Dalton's formulation (11) and contained the following: NaCl, 465 mM; KCl, 10 mM; $CaCl_2$, 25 mM; $MgCl_2$, 4 mM; $MgSO_4$, 4 mM; Tris-HCl, 5 mM.

Computations were carried out on a Control Data Cyber 73 computer at the Computer-based Education Research Laboratory (CERL) at the University of Illinois (Urbana, Ill.) and on a similar system at Control Data Corporation in Minneapolis, Minn. Access to the computer was through a remote "Plato IV" terminal developed by CERL. A second-order, modified Euler predictor-corrector method (see 2) was used for the numerical integrations of the expanded Hodgkin-Huxley equations. Parallel mode integration was used. The standard word length carried by the system was 60 bits, giving 14 places for floating point variables. A time increment of 25 μs was used. This value resulted primarily as a carry-over from earlier simulations in which 6.3°C Hodgkin-Huxley parameters were used and in which a close duplication of the FitzHugh-Antosiewicz simulation (14) was made as an accuracy check. Several examples of single action potentials and multiple action potentials were run both at 25 μs and at 10-μs steps with 18°C parameters to check for the types of computational errors pointed out by Moore and Ramon (28). The results matched for the different step sizes to approximately a line width of the display unit. At the other extreme, solutions in which voltage changed very slowly were duplicated for 25- and 75-μs steps to check for changes in the voltage trajectory that might indicate round-off errors. In this study all time constants in the Hodgkin-Huxley equations were scaled to 18°C.

EXPERIMENTAL RESULTS

Sodium Conductance

With respect to the sodium transient, there is little difference in the appearance of raw voltage-clamp data from the crustacean leg axons and model preparations such as squid axon and amphibian node of Ranvier (*c.f.* 20, 12). The sodium conductance will be described with the standard Hodgkin-Huxley (22) formalism; $g_{Na} = \bar{g}_{Na} m^3 h$. $\bar{g}_{Na}$ is a normalization factor, m and h are functions of membrane voltage (V_m) and of time which vary between 0 and 1. The steady-state values of these parameters (m_∞, h_∞) are of particular importance to the study. A comparison of these parameters derived from walking leg axon data and the parameters of the Hodgkin-Huxley axon is given in Fig. 1. The data points in this figure were obtained from walking leg axons of both *Callinectes* (Fig. 1A) and *Cancer* (1B) in a manner similar to that described by Hodgkin and Huxley (20, 21) except that TTX (3×10^{-7}M) was used as a blocking agent to obtain the separated sodium transient. For a step to a given voltage, the time-course of the sodium transient was obtained by subtracting currents recorded in control and TTX saline. The falling phase of the sodium current was plotted on semilog paper and fit by eye to a straight line. The zero time intercept was determined and this procedure was repeated for a number of voltage steps covering a range from −40 mV to approximately +30 mV. Currents were converted to conductances by the expression $g_{Na} = (I_{Na}/(V_m - E_{Na})$, where E_{Na} is the sodium equilibrium potential and V_m is the voltage at which current is measured. The m_∞ curve is a plot of the normalized conductance intercept vs. the value of the test step. In some axons the decay

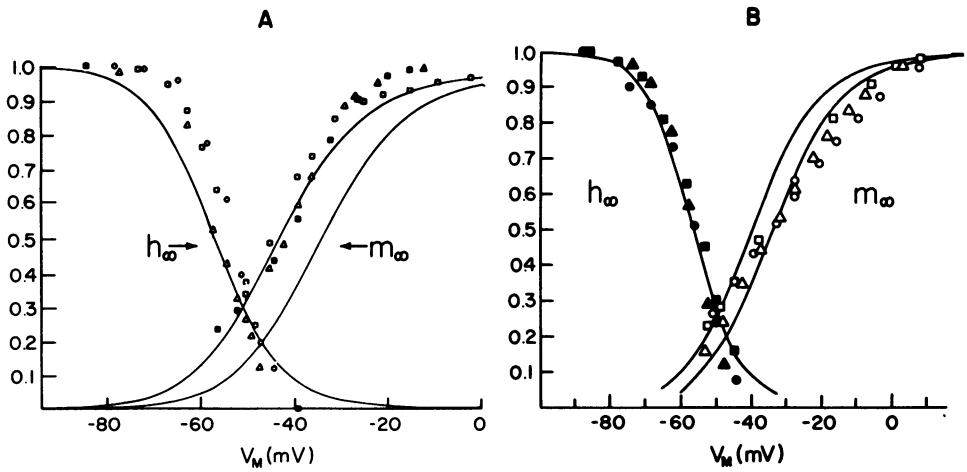

FIGURE 1 Steady-state parameters (m_∞ and h_∞) of the Na conductance system for crab axon preparations; A: *Callinectes;* B: *Cancer.* Data points are shown for three preparations each. Characteristics of the Hodgkin-Huxley axon are shown by the continuous curves. The squid h_∞ was made to overlay the pooled crab data. To achieve a moderate fit to the crab data, the squid m_∞ curve must be shifted 9 mV in A and about 6 mV in B.

time-course of I_{Na} for small voltage steps was not well fit by a single exponential (see 7). This complication was ignored in the present analysis.

The h_∞ curve was determined in experiments where V_m was stepped from rest to a conditioning voltage (the experimental variable) for 40 ms and then to a fixed test voltage. For a given experiment the test voltage chosen was the one that gave maximum I_{Na}. The normalized peak in I_{Na} was then plotted vs. conditioning voltage to give the h_∞ curve.

In Fig. 1 the squid axon h_∞ curve has been made to overlay the analogous data points for the crustaceans in the voltage region around threshold. The squid axon m_∞ curve and the crab data points clearly do not overlay in this arrangement. However, a rather good fit is achieved if, in Fig. 1A, the squid m_∞ curve is shifted 9 mV to the left, increasing the overlap between the two curves so that the intersection of the m_∞ and h_∞ curves becomes approximately 0.3 instead of its original 0.2. For *Cancer* (1B) the intersection is at a lower point and the necessary shift is less. The voltage dependence for *Cancer* is also less steep. For the *Cancer* m_∞ data (Fig. 1B) the fit to the larger data points is made worse by the shift. This trade-off was made because repetitive activity is being considered and the values of parameters near threshold are more important than those at larger depolarizations. The differences in the *Callinectes* and *Cancer* data may be due in part to the series resistance compensation used in experiments on *Cancer* but not in earlier experiments on *Callinectes*. One of the effects of series resistance is to increase the magnitude of I_{Na} at small to intermediate depolarizations and decrease it at large depolarizations, altering the shape of the m_∞ curve. The shifting operation gives rise to less sodium conductance inactivation at threshold values of membrane voltage in the crab axons even for voltage trajectories that approach threshold very slowly. Such a finding is not without precedent in the literature. Vallbo (34), in a comparative study of rapidly and slowly accommodating nodes of Ranvier, showed that the h_∞ parameter of the sodium system was displaced to the right by several millivolts in the slowly accommodating fibers as compared to the rapidly accommodating ones. Assuming that the m_∞ parameter was invariant between the two fiber classes, as was done in a subsequent modeling study (16), would indicate a greater region of overlap of m_∞ and h_∞ in the slowly accommodating fibers. Also, it is well known that squid axon becomes more oscillatory in low-calcium medium (25) and it has been shown that one of the effects of low calcium on the sodium conductance is to shift the voltage dependence of m_∞ and h_∞ to the left. However, m_∞ is a more sensitive function of external calcium than is h_∞ (cf 29), and in low calcium the overlap of the two curves is greater than normal. The m_∞ and h_∞ overlap is also greater in the repetitive neurons of *Anisodoris* than in the Hodgkin-Huxley axon. If the data of Connor and Stevens (9) are put into suitable form, the intersection point of m_∞ and h_∞ for their exemplar cell is approximately 0.3.

It should be noted at this point that some studies have indicated that the voltage dependence of h_∞ is affected by differences in the measurement protocol. That is: the position but not the shape of the h_∞ curve on the voltage axis depends to an extent

upon the value of the test voltage. The matter has been examined at length by Hoyt and Adelman (24) in the squid and Goldman and Schauf (18) in *Myxicola*. Such an effect is not appreciable in repetitive crustacean axons (7).

To complete the description of the sodium conductance system for computation, the squid axon activation and inactivation time constants τ_m and τ_h were shifted by the same voltage as the steady-state parameters. For the simulations shown, a low value of $m_\infty - h_\infty$ intersection (0.27) was used. Expressions used in computations are given in the Appendix A.

Potassium Conductance

A general description of potassium currents has been given in a previous article (6). There are two components of outward current in the repetitive fibers: a delayed component qualitatively similar to the squid axon potassium current I_K, and a second component that is at least to a large extent a transient current, I_A. Fig. 2 shows raw data from what will be considered a model axon. At the two smallest voltage steps the steady-state current can be accounted for by assuming a constant leakage conductance. That is, the steady-state currents plot on the same straight line as the currents for small, nonactivating steps. The time-course of current decay to the steady-state

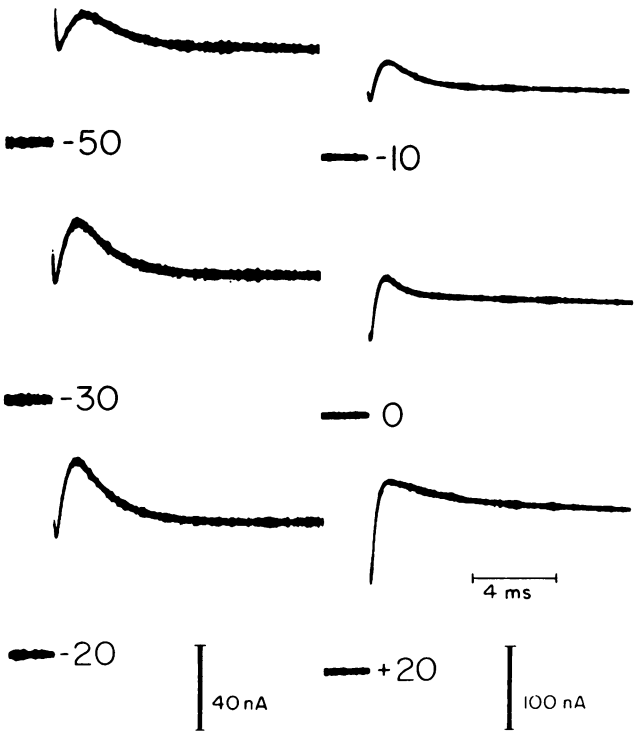

FIGURE 2 Raw data from a repetitive axon demonstrating two-component outward current with I_A predominating. Saline contained 3×10^{-7} M TTX. Value of the test voltage is shown by each current trace. Holding voltage = −100 mV.

value follows a single exponential. For larger voltage steps the steady-state current becomes much larger than leakage current and the decay time-course is no longer exponential. The change in characteristics at larger voltage steps is largely due to activation of the maintained current, I_K. To obtain a quantitative expression for the transient I_A, the following procedures were used. First an estimate of the I_A inactivation time constant, τ_B, was obtained. For voltages where the steady-state current was less than 30% of the peak outward current, the time constant of total current decay to its steady-state value was used. At more positive test voltages where I_K was larger, values were determined as follows: The time-course of I_K was determined by holding the membrane voltage between test pulses at a value positive enough to inactivate I_A (see Fig. 8 of ref. 6) and stepping to more positive levels. Total current in this case should be $I_K + I_L$ (delayed potassium plus leakage current). For more negative holding potentials the current record should consist of $I_A + I_K + I_L$ and the difference between two such current waveforms at the same test voltage should yield I_A. The subtraction method is not highly reliable since it puts considerable emphasis on small differences between fairly large currents. In practice it was necessary to scale up the traces from the more positive potential to attain equal steady-state values of current (see also 8). In scaling the current in this manner, it is assumed that the smaller values I_K attains for more positive holding potentials are due to a slow inactivation process operating on I_K and not to some other factor affecting a steady-state value of I_A. We have not been able to devise an adequate means of testing this assumption but it seems a reasonable working hypothesis. Values for τ_B and time to peak outward current for three preparations are given in Fig. 3A. Where contamination by I_K was least, at small

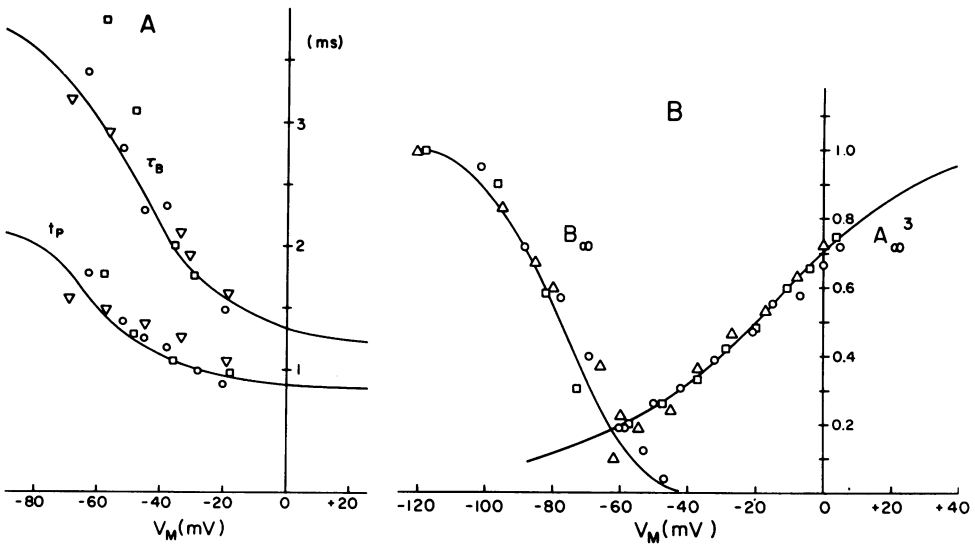

FIGURE 3 I_A system parameters vs. membrane voltage. A: inactivation time constant, τ_B; time to peak current, t_p. B: steady-state activation, A_∞^3; steady-state inactivation, B_∞. Continuous curves drawn from expressions in Appendix.

depolarizations, the best measure of τ_B was probably obtained, although here the total current excursion was small, introducing reading error as a factor limiting accuracy. The simulation section will show that the values of τ_B in this region are the most important in determining repetitive activity. At intermediate depolarization the total current decay gives a sizeable underestimate of τ_B, since the steady-state current is made up largely of the slowly activating I_K instead of the leakage current. Therefore, the relationship of τ_B to V_m shown in Fig. 3A is probably steeper than it should be. These approximate measures used to determine τ_B were justified because the number of experimental measurements necessary on this short-lived preparation were relatively few and because they gave low values of τ_B, which biased the simulations toward poor model performance at low firing frequencies.

Conductance data for the I_A system were cast into a form identical to the Hodgkin-Huxley sodium conductance formulation (22), i.e. $g_A(V,t) = \bar{g}_A A^3 B$, where $\bar{g}_A$ is a normalization factor, A an activation term, and B an inactivation term. For a positive-going voltage step from a large negative holding potential into the range where I_A is activated, the expression for the conductance time course is:

$$g_A(v,t) = \bar{g}_A\{A_\infty(v)\left[1 - e^{-t/\tau_A}\right]\}^3 B_0(v)\left[e^{-t/\tau_B}\right]$$

$B_0(v)$ was determined from variable holding experiments described in a preceding paper (see Fig. 9 of ref. 6). The parameters $\bar{g}_A$, $A_\infty(v)$, and τ_A were evaluated by fitting the peak value and time to peak of g_A at voltages throughout its range of activation. Partially complete runs from 12 fibers were available for analysis. Data from three fibers which had the greatest degree of consistency and completeness have been pooled to

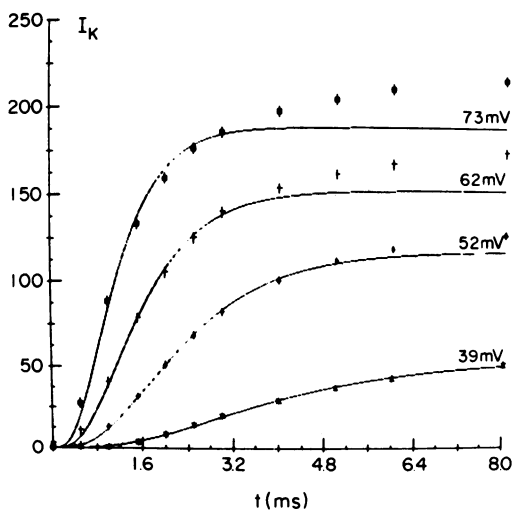

FIGURE 4 Crab axon delayed potassium currents for a family of voltage steps (data points) and best fit obtainable by a fourth-power exponential (continuous curves). Voltage step size is given at the right side of each trace. Current intensity is given in nano amperes.

give the data used in computation and are shown in Fig. 3. Fitting expressions used in the simulations are given in the Appendix.

A modified form of the Hodgkin-Huxley description of I_K for the squid axon was used to approximate the crab axon I_K data. Modifications were guided by the following experimental findings: first, there is little activation of I_K at sub- and near-threshold voltages; second, at small to intermediate depolarizations the kinetics are slower than squid; and third, the magnitude of I_K relative to I_{Na} is smaller. Fig. 4 illustrates a family of delayed outward currents from a walking leg axon (data points). The holding potential was positive enough, approximately -50 mV, that the I_A system was inactivated. The smooth curves represent a fourth-power exponential fit to the data. At intermediate depolarizations the fit is adequate but for the larger currents a slow activation process causes the later data points to deviate from the fourth-power approximation. The curves shown were generated by fitting only the initial points of the I_K time-course at the larger voltages. This slowly activating feature has been ignored in the computational section. Time constants are given in Fig. 5.

Activation of I_K at small voltage steps was reduced by shifting the steady-state activation parameter, n_∞, 4.3 mV to the right along the voltage axis and the current amplitude was reduced by changing $\bar{g}_K$ from its standard value of 36 to 20. This overprecise shift value was used to give an optimally flat I-V relationship in the steady state (see Fig. 8). Parameters are summarized in the Appendix. With these changes in the delayed potassium system and the inclusion of I_A, the outward current pattern of

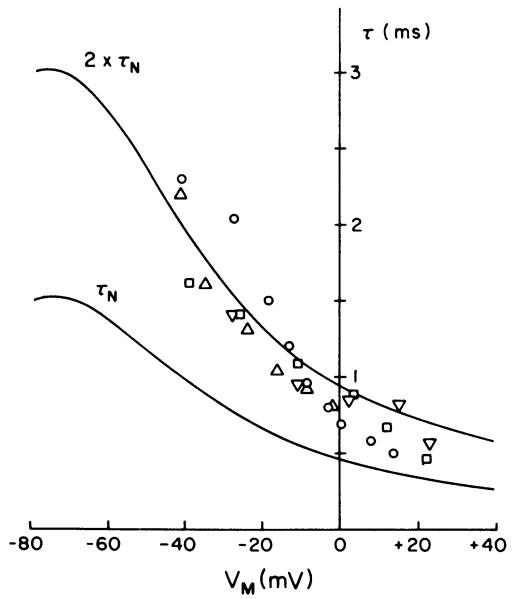

FIGURE 5 A comparison of crab axon τ_n (fourth-power fit) to squid axon τ_n at 18°C. Data from four preparations were pooled. Upper curve labeled 2 × τ_n was constructed by scaling the squid τ_n by a factor of 2 (18°C parameters).

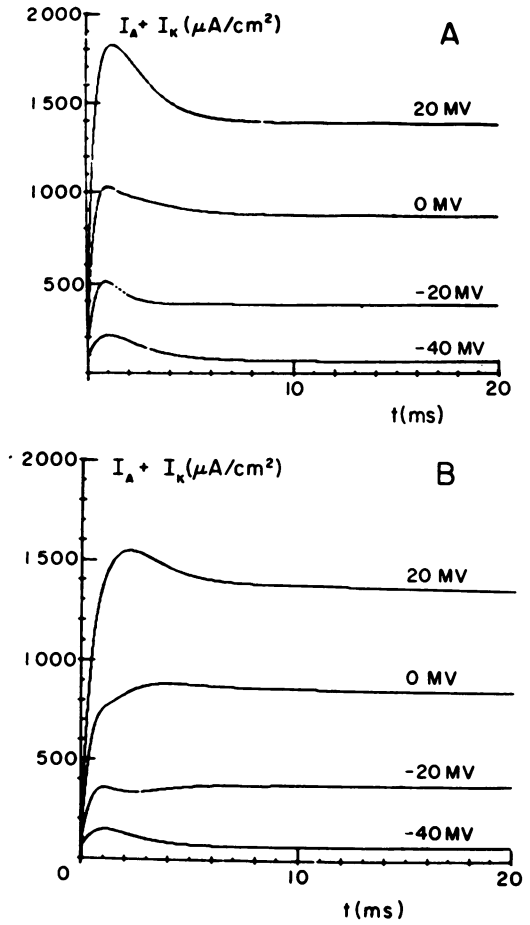

FIGURE 6 Simulated potassium currents ($I_A + I_K$) under voltage clamp. A: g_A = 47.7 mmho/cm^2. B: g_A = 33 mmho/cm^2. Other conductance parameters given in text. Holding voltage = −100 mV.

repetitive walking leg axons can be matched reasonably well except at large depolarizations, where the I_A components are too prominent. Fig. 6 shows two families of computed voltage clamp currents for $I_K + I_A$, with the modifications in I_K discussed above. In Fig. 6A the value of $\bar{g}_A$ was set to 47.7 mmho/cm^2 (its experimentally determined value) and $\bar{g}_K$ was set to 20 mmho/cm^2. The curves should be compared to the experimental data shown in Fig. 2. There is a considerable gradation in the relative magnitudes of $I_A + I_K$ between fibers (see ref. 6) and in Fig. 6B, $\bar{g}_A$ was reduced to 33 mmho/cm^2 while $\bar{g}_K$ was left at 20. The total current corresponds to records taken from intermediate fibers. For the computations to follow, the standard value of $\bar{g}_A$ is taken as 47.7. A number of examples have also been run for $\bar{g}_A$ = 33 and have illustrated that this change has relatively minor effect upon the minimum repetitive firing interval but does decrease threshold stimulus current.

COMPUTATIONAL RESULTS

Modified Four-Branch Model

Before the computations involving the full model, the effects of modifying only the squid axon sodium and potassium systems in the manner indicated are demonstrated. In this set of simulations the usual four parallel branches were employed, i.e. sodium, potassium, and leakage conductances plus membrane capacitance. See Appendix for details. Fig. 7 shows the response of the four-branch equivalent circuit, $\bar{g}_A = 0$, to applied constant current of two different amplitudes, one just above threshold and the other just sufficient to evoke a repetitive train. The most significant difference between these records and a repetitive train from the Hodgkin-Huxley axon or node of Ranvier (*c.f.* 32, 3) is that all the action potentials are full-sized. This is a direct consequence of the increased overlap of the m_∞ and h_∞ curves (see also 27, 35). Even with the weakened potassium system, the later spikes of simulated trains were shorter than the first when there was normal overlap of m_∞ and h_∞. Other differences are minor and directly in accord with the changes made in the potassium system parameters. That is, the action potentials have a greater duration than the standard model and the minimum firing rate is somewhat lower. Simulations in which the sodium conductance parameters were varied showed that these effects are due primarily to the weakening and slowing of the potassium conductance system. The firing pattern observed is otherwise qualitatively the same as that exhibited by the Hodgkin-Huxley axon. Repetitive firing has a definite minimum firing frequency, which is large, approximately 77 spikes/s. The dynamic frequency range is small as a result and there is a

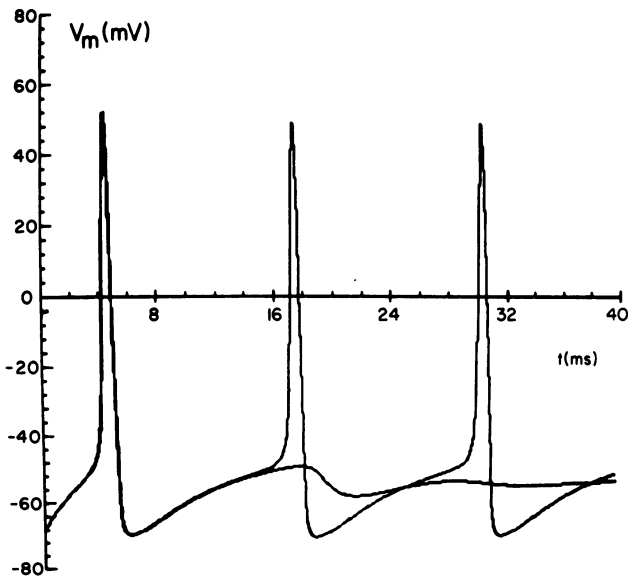

FIGURE 7 Response of four-branch equivalent circuit ($g_A = 0$) to constant current stimuli. I_{stim} = 7.4 $\mu A/cm^2$ fired one spike; I_{stim} = 7.5 fired an infinite train.

pronounced tendency towards subthreshold oscillation. It should be noted that E_L has been adjusted so that the rest potential is -68 mV instead of the normal -60 mV. This has been done to facilitate comparison with later records. Nearly identical results to Fig. 7 were obtained with E_L adjusted to give a rest potential of -60 mV.

Five-Branch Model

The first effect noted of inserting the I_A system into the axon model was an increase in the resting potential to a value very close to E_K when the leakage battery was set at its normal value, -49.4 mV. The reason for this is most effectively explained in terms of a plot of the steady-state values of each of the component membrane currents (see Fig. 8). Because of the way the A_∞ and B_∞ curves overlap (see Fig. 3), there is a voltage range where the steady-state value of g_A increases with increasingly negative membrane voltage. The rate of this increase is large enough that I_A increases over a portion of the range even though the driving force (V-E_K) is decreasing. At E_K, I_A falls abruptly to zero. At steady-state or rest, the membrane voltage will be that value for which the different membrane currents, primarily I_A and I_L, sum to zero. For V_L = -49.4 and g_L = 0.3 the approximate value is -72 mV. Holding g_L constant but lowering the value of E_L towards zero moves the resting potential in a positive direction. A standard resting potential of -68 mV has been employed for most subsequent calculations. The corresponding E_L is -17 mV. Starting a response from voltage levels more negative than -68 mV has a large effect on the amount of stimulus necessary to drive the membrane potential "up the hill" to threshold but has relatively minor effect upon the frequency of the repetitive response except at very low values of g_L. The

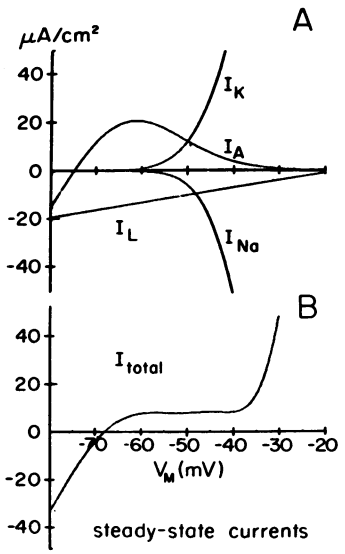

FIGURE 8 A: Steady-state value of individual ion currents vs. voltage of the five-branch model with standard parameters. B: Steady-state total membrane current vs. voltage plotted to same scale as A.

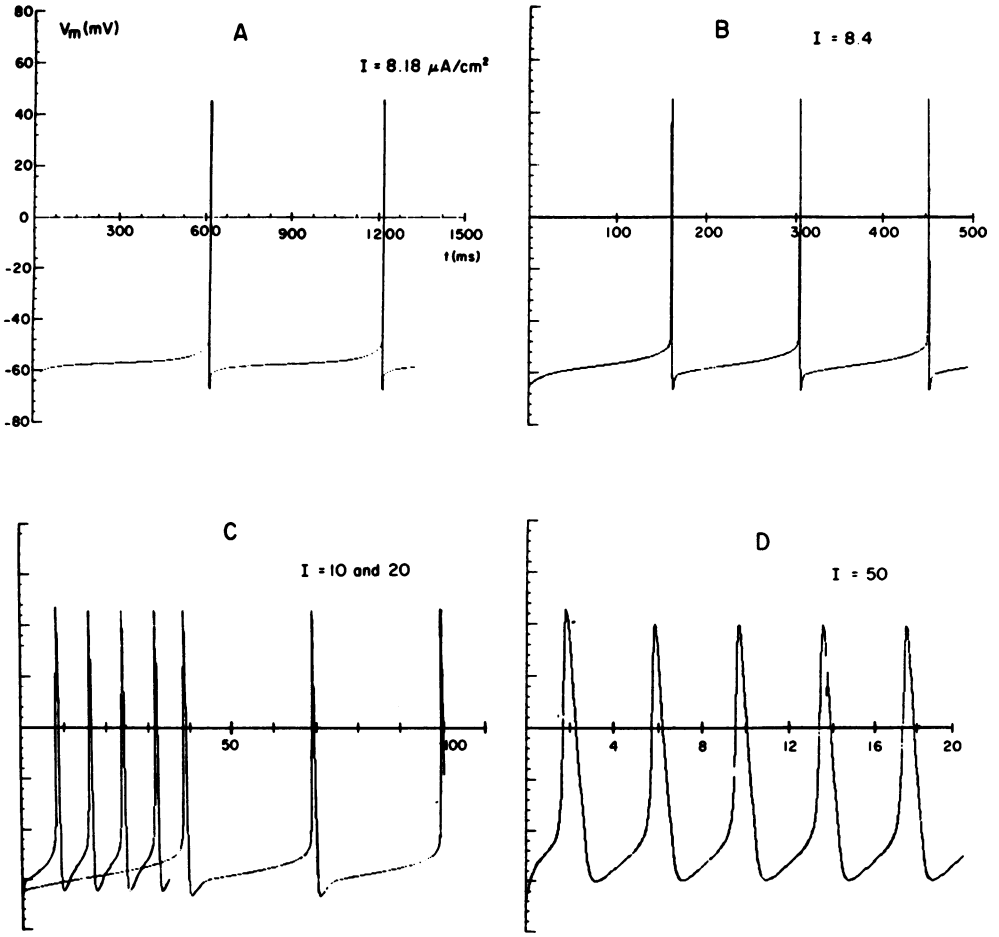

FIGURE 9 Firing pattern of standard model. Values of stimulus current shown in each panel.

I-V curve for the standard model is given in Fig. 8B. Tomita and Wright (33) and Chapman (4) have reported significantly higher resting potentials in repetitive-firing axons than in the nonrepetitive ones. This observation is certainly consistent with the scheme shown here since repetitive axons (classes I and II) have an I_A system whereas nonrepetitive ones (class III) do not, but whether this is coincidence or not is uncertain.

The response of the complete model to a small depolarizing current is shown in Fig. 9 A. The lower bound for repetitive firing was under 2 spikes/s at a current of 8.18 $\mu A/cm^2$. A current stimulus of 8.16 $\mu A/cm^2$ gave a subthreshold response. Finer tuning of the current intensity is unrealistic, in view of noise considerations in real systems, as well as expensive. That is, there might be a stimulus value for which there would be only one action potential fired by the model, but the number of decimal places necessary in the value of stimulus current would probably be below the noise level of an experiment. Fig. 9 B, C, and D demonstrate the response trains to larger

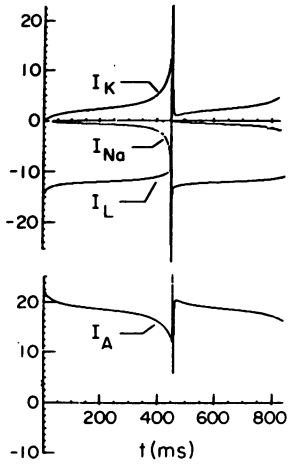

FIGURE 10 Plot of ion currents underlying the firing pattern of Fig. 9. Ordinate scales are the same in upper and lower panels, $\mu A/cm^2$.

stimulus currents. The maximum firing frequency of the model was approximately 350 spikes/s. At the higher frequencies the response after the first spike tended to be more a damped oscillation than action potentials. Since the mechanisms generating low frequency response are of primary concern here, the high frequency behavior has not been examined closely.

The ion currents that flow in response to a small depolarizing current step are detailed in Fig. 10. I_A and I_L start with equal and opposite values, since both I_{Na} and I_K are initially zero. After the stimulus current is switched on, I_A undergoes a quick, transient increase and then proceeds to decrease slowly and continues to do so as time progresses even though the driving force for I_A increases. I_{Na} and I_K become appreciable later and increase for the duration of the latent period. I_K is the larger of the two, however, and the net effect of these two currents alone is to repolarize the membrane. The voltage trajectory is then determined by the joint action of the three dynamic conductance systems and the membrane capacitance, but the controlling factor is the I_A system. The importance of minimizing the activation of I_K at subthreshold voltages should be clear from this figure since a stronger I_K activation would offset the I_A decrease and there would be no rising voltage trajectory. The voltage rate of change increases near threshold as I_A drops more sharply and I_{Na} begins its precipitous increase. Both I_A and I_{Na} are involved in generating this part of the voltage trajectory. The time course of currents during the action potential are off scale and will not be examined here. During the spike after-potential, the parameters of the I_A and I_{Na} systems are reset to values near their initial ones and a similar cycle is begun.

The interaction between I_A and I_K during the spike after-potential is very important in determining the next interspike interval. Factors that reduce or quicken the undershoot shorten the interval. An example is given in Fig. 11 A, where the spike under-

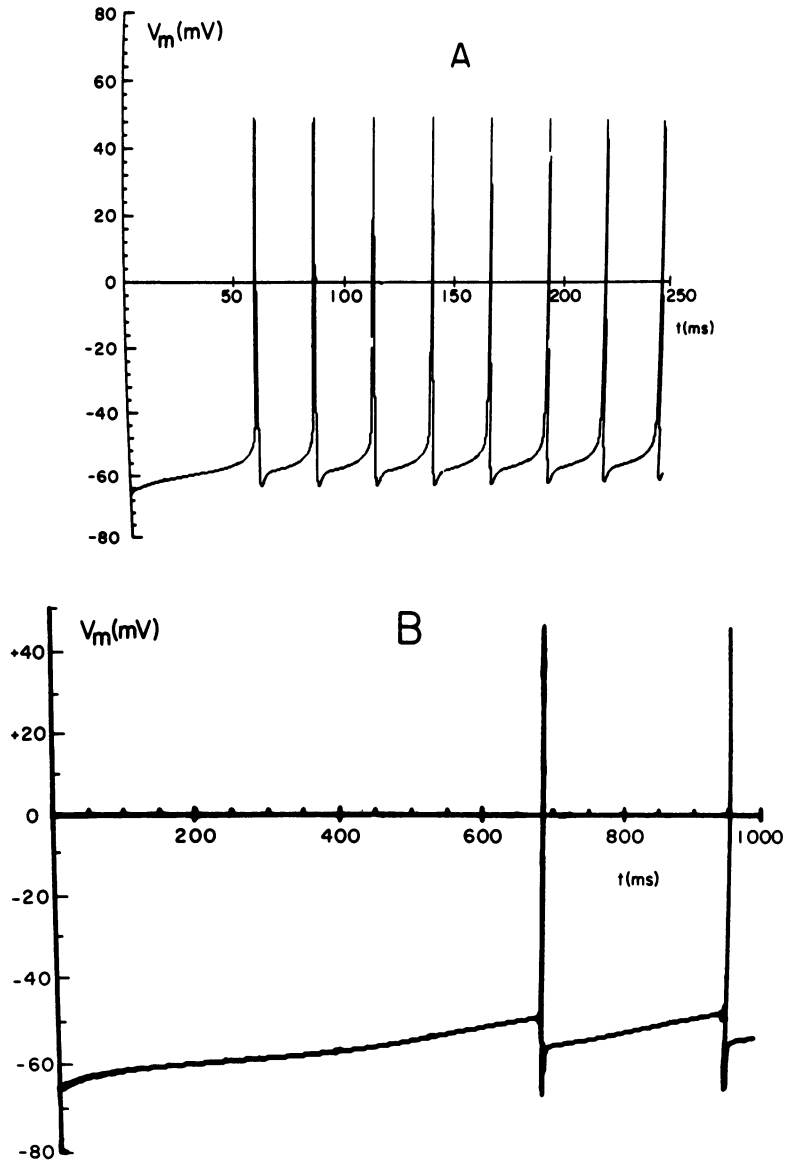

FIGURE 11 A: Repetitive activity showing the effect of reducing $\bar{g}_K$ by a factor of 2. B: Response showing the effect of multiplying τ_B by a factor of 3 with all other parameters standard. Stimulus 8.4 $\mu A/cm^2$.

shoot has been reduced by cutting $\bar{g}_K$ from 20 to 10 mmho/cm^2. The shallow undershoot allows less reactivation of the I_A system and its large initial value is never regained. Consequently the amplitude of I_A after the first and later spikes is small and the second and all following interspike intervals are much shorter than the first. A somewhat similar result obtains if τ_n is reduced. Conversely, if τ_B is increased, the

interval preceding the first spike, sometimes called the utilization time (19), is increased almost proportionately at a given stimulus current intensity. Quite long utilization times can be achieved by moderate increases in τ_B. In the example shown in Fig. 11 B, the τ_B function was multiplied by three. The maximum value of τ_B for this simulation was still only 10 ms on the voltage range covered by the prespike trajectory. The interspike interval, however, is shorter than if τ_B were left at its standard value because, as in Fig. 11 A, the I_A system only slightly recovers during the spike undershoot, this time because of its own slow kinetics.

The characteristics of the voltage trajectory where only I_A, leakage, and capacitive currents are present are shown in Fig. 12. The magnitude of stimulus current has been reduced because it is not necessary to counteract the effect of I_K activation. It is clear that the reduced system is capable of generating a very slow, ramp-type depolarization when presented with a constant current stimulus. Over the middle portion of the voltage trajectory the system responds as a fairly good integrator. A feature not noticeable in simulations where all currents are active is the upward break in the voltage trajectory as I_A inactivates completely. Normally this upward break would carry the voltage to threshold and the effect would be immediately obscured by the much larger I_{Na} and I_K.

The responses shown in Fig. 9 correspond very closely to class I repetitive activity reported by Hodgkin (19) and Chapman (4) in crustacean leg axons. The frequency range of the model in the form presented is over 100:1, comparable to what is observed experimentally in a variety of repetitive neurons. A plot of firing frequency vs. stimulus intensity is given in Fig. 13.

In appearance, the model responses shown in Fig. 11 are similar to Hodgkin's class II repetitive activity, characterized by a long utilization time and a high minimum

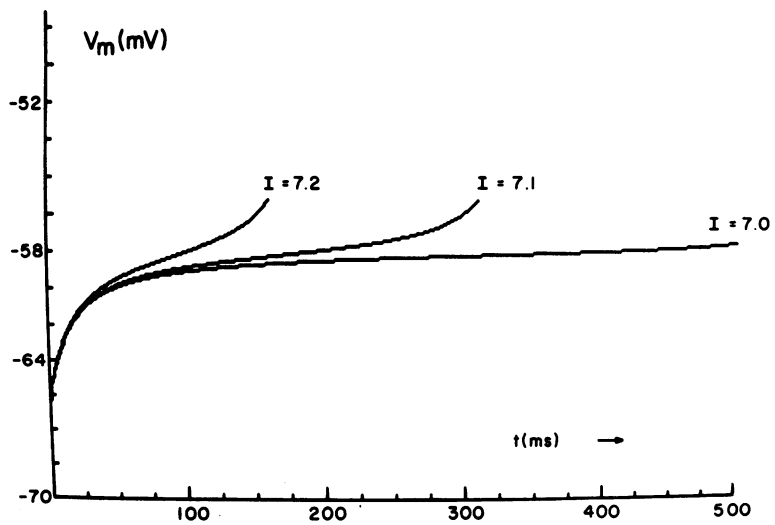

FIGURE 12 Voltage trajectories generated by constant currents of 7.00, 7.11, and 7.2 $\mu A/cm^2$ applied to the leakage, capacitive, and I_A branches of the standard model.

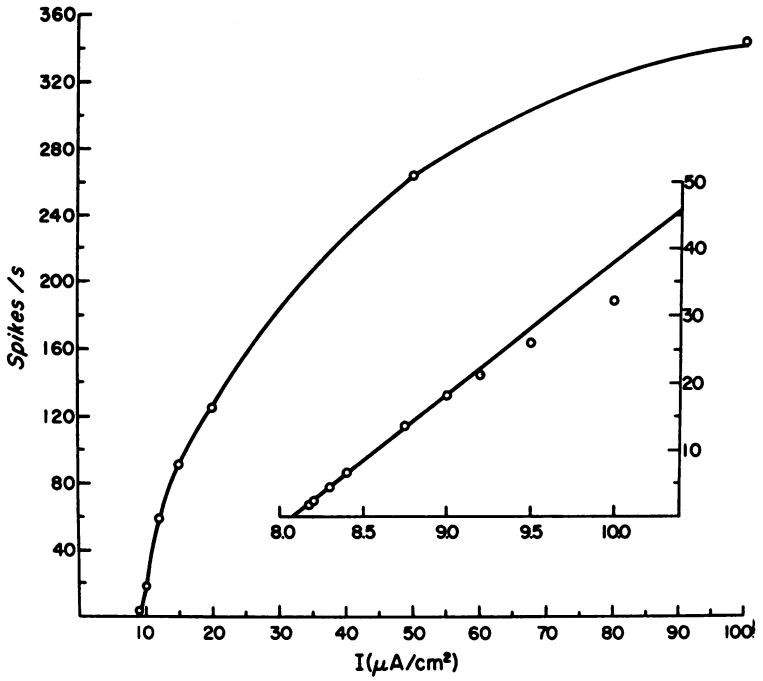

FIGURE 13 Plot of repetitive firing frequency vs. stimulus current magnitude for the standard model. Expanded view of the lower frequency range is shown in the inset.

repetitive rate. Whether the mechanism underlying the variation in response is a reduction in the ratio of τ_n:τ_B, a reduction in the ratio of $\bar{g}_K$:$\bar{g}_A$, or a third unknown possibility has not been determined.

It was noted in the preceding paper (6) that certain conditions attendant upon the double sucrose gap were not favorable to repetitive firing, notably, high g_L and the large steady hyperpolarization. These conditions have been modeled by increasing g_L to 2 mmho/cm^2 and by moving E_L to -115 mV. In effect a second leakage branch has been added to the equivalent circuit, one arising because of conditions in the experimental chamber, and in comparison the original leakage branch is unimportant. The model behavior is similar to experimental observations: threshold stimulus is very high, there is no low frequency discharge, and the subthreshold voltage response displays an upward creep.

DISCUSSION

The most significant outcome of this analysis is the demonstration that integration times of the order of hundreds of milliseconds can be achieved in membranes under space-clamped conditions by conductances that have relaxation times of less than 5 ms. At first this would seem to imply that the low-frequency behavior is governed not by dynamic conductance changes but by their steady-state characteristics, since there is such a disparity in time scales. That is, the slow ramp of Fig. 12 generated by capac-

itance, leakage, and I_A branches would not be due so much to the time dependence of g_A decay but more to the fact that g_A decreases with positive-going V_m over the voltage range covered. This idea was tested by performing simulations with τ_A and τ_B reduced by a factor of 10 over the entire voltage range. This operation had negligible effect on the shape of the action potential but drastically increased the minimum firing frequency. (Increasing τ_B also increased utilization time, as noted in Fig. 11.) These results demonstrate that both the dynamic and steady-state characteristics are important in generating the slow response. At any given voltage on the way up the ramp to threshold voltage, g_A finds itself at an inappropriately high value and decreases, forcing the voltage under constant current stimulation still farther up in a form of reverse bootstrapping operation.

The presence of a flattened (high resistance) region in the steady-state *I-V* relationship (see Fig. 8) is also critical. This factor has been pointed out previously by Hodgkin and modeled in a different fashion from that shown here by Dodge (13). For example, increasing the minimum slope of the *I-V* relation by 0.5 μA/mV-cm^2 can reduce the maximum interspike interval to a value between 100 and 200 ms. The change in slope can be brought about by an increase in g_L or a decreased shift of potassium parameters. A negative slope region, generated by an increase in m_∞-h_∞ overlap, does not cause serious degeneration of the low-frequency response but does cause the frequency to become a steeper function of stimulus intensity. A systematic study of this type of variation has not been made. The slow repetitive response therefore depends upon a touchy balance of a number of parameters and is easily disrupted. This should come as no surprise since it is certainly the most labile electrophysiological response of a living neuron.

Considered from a general systems standpoint, the model is quite a reasonable design for a current-to-frequency converter. The dynamic range is large and there is a considerable region where the output-to-input relation is linear. A more subtle aspect is that the system is fairly insensitive to noise because the individual currents that control the interspike voltage trajectory are large (see Fig. 10) and the I_A system tends to be self-correcting for spurious inputs. That is, if a positive or negative noise pulse were superimposed upon a steady background current, the resulting increase or decrease in A, which has a small time constant, would produce an appreciable opposing current that would damp the disturbance.

There are several important aspects of repetitive activity, both in the crustacean leg axon and in other preparations, that this simulation does not account for. With respect to crustacean axons the action potential duration is too long due to a slow falling phase, a repetitive train does not show adaptation, and a very high frequency train does not damp out as quickly as is actually observed. Many repetitive neurons, but not the crustacean axons, also exhibit utilization times short in comparison to the interspike interval. The first set of deficiencies is at least partially traceable to the errors in fitting the delayed potassium conductance data mentioned in the Results section. The I_K system used in the computations is weaker at positive voltages then it should be because a slowly activating component present in the voltage clamp data was dropped

out of the description (see Fig. 4). Also, separation of I_K and I_A components at large depolarizations was subject to uncertainties that may have introduced amplitude or time-course errors into the model. Either of these types of errors might lengthen the downstroke of the action potential by resulting in less activation of the I_K system in the model than actually exists. With respect to accomodation, the slowly activating component, omitted in the simulation, might be expected not to reach a steady-state cycle within the time of the first few action potentials of a train, especially at high frequency firing. This current would then be expected to build up a steady activation during the initial part of a train which would counterbalance part of the stimulus current and lead to a reduced firing rate. A similar mechanism has been demonstrated by Partridge and Stevens in molluscan neurons (30).

The long utilization times, a rather atypical feature of crustacean axons with respect to other repetitive neurons, arise from the significant overlap between the A_∞ and B_∞ curves and the fact that the resting potential lies in this region. In *Anisodoris* central neurons, where the utilization time is generally short compared to the interspike interval, there is very little overlap between the A_∞ and B_∞ curves, and B_∞ is very small at the resting potential (8).

The simulations presented here must be regarded as formal since not all of the parameters of the specific system, crustacean axons, fit well into the model axon mold. This carries the disadvantage that some parameter may be defined improperly, for example, sodium and potassium conductance activation. Wherever the data fit was imprecise we have tried to make our estimates to the side of the worst model performance or else we have made simulations using parameter values that "bracket" the range over which the parameters lie. An advantage of this type of approach, other than those given in the introductory section, is that it illustrates more strongly than others the minimal requirements for the generation of long integration times in space-clamped systems.

We are indebted to Professor A. O. D. Willows, Director of the Friday Harbor Laboratories, for making available the facilities of the laboratories during portions of this investigation and to Professor Frederick A. Dodge for suggesting helpful changes in the simulations. We would also like to acknowledge the help of B. Nelson, K. Murphy, and A. Prickett in preparing the manuscript, and the generosity of the Computer Based Education Laboratory and Control Data Corporation for the use of computer time and facilities.

This study was supported by GB-39946 from the National Science Foundation, Biomedical Science grant RR-07030 from the School of Life Sciences at the University of Illinois, and a Grass Foundation fellowship during the initial part of this study.

Received for publication 4 October 1976 and in revised form 16 December 1976.

REFERENCES

1. AGIN, D. 1964. Hodgkin-Huxley equations: logarithmic relation between membrane current and frequency of repetitive activity. *Nature. (Lond.).* **201**:625–626.
2. BECKETT, R., and J. HURT. 1967. Numerical calculations and algorithms. McGraw-Hill Book Company, New York. 193–198.
3. BROOM, B., and B. FRANKENHAEUSER. 1972. Repetitive discharge of excitable membrane computed on the basis of voltage clamp date for the node of Ranvier. *Pflugers Arch. Eur. J. Physiol.* **332**:21–27.

4. CHAPMAN, R. A. 1966. The repetitive responses of isolated axons from the crab *Carcinus maenas*. *J. Exp. Biol.* **45**:475–488.
5. COLE, K. S., and J. W. MOORE. 1960. Potassium ion current in the squid giant axon: dynamic characteristic. *Biophys. J.* **1**:1–14.
6. CONNOR, J. A. 1975. Neural repetitive firing. A comparative study of membrane properties of crustacean walking leg axons. *J. Neurophysiol.* **38**:922–932.
7. CONNOR, J. A. 1976. Sodium current inactivation in crustacean axons. *Biophys. J.* **16**:24a. (Abstr.).
8. CONNOR, J. A., and C. F. STEVENS. 1971. Voltage clamp studies of a transient outward membrane current in gastropod neural somata. *J. Physiol. (Lond.).* **213**:11–30.
9. CONNOR, J. A., and C. F. STEVENS. 1971. Prediction of repetitive firing behavior from voltage clamp data on an isolated neuron soma. *J. Physiol., (Lond.).* **213**:31–54.
10. CONNOR, J. A., D. WALTER, and R. MCKOWN. 1974. Neural repetitive firing. Modifications of the Hodgkin-Huxley axon suggested by experimental data. *Fed. Proc.* **33**:1266. (Abstr.).
11. DALTON, J. C. 1958. The effects of external ions on membrane potentials of a lobster giant axon. *J. Gen. Physiol.* **41**:529–542.
12. DODGE, F. A., and B. FRANKENHAEUSER. 1958. B. Sodium currents in the myelinated nerve fibre of *Xenopus laevis* investigated with the voltage clamp technique. *J. Physiol. (Lond.).* **148**:188–200.
13. DODGE, F. A. 1972. On the transduction of visual, mechanical, and chemical stimuli. *Int. J. Neurosc.* **3**:5–14.
14. FITZHUGH, R., and H. A. ANTOSIEWICZ. 1959. Automatic computation of nerve excitation. Detailed corrections and additions. *J. Soc. Indust. Appl. Math.* **7**:447–458.
15. FRANKENHAEUSER, B., and A. F. HUXLEY. 1964. The action potential in the myelinated fiber of *Xenopus laevis* as computed on the basis of voltage clamp data. *J. Physiol. (Lond.).* **171**:302–315.
16. FRANKENHAEUSER, B., and A. B. VALLBO. 1965. Accommodation in myelinated nerve fibres of *Xenopus laevis* as computed on the basis of voltage clamp data. *Acta Physiol. Scand.* **63**:1–20.
17. FUORTES, M. G. F., and F. MANTEGAZZINI. 1962. Interpretation of the repetitive firing of nerve cells. *J. Gen. Physiol.* **45**:1163–1179.
18. GOLDMAN, L., and C. L. SCHAUF. 1972. Inactivation of the sodium current in *Myxicola* giant axons; evidence for coupling to the activation process. *J. Gen. Physiol.* **59**:659–665.
19. HODGKIN, A. L. 1948. The local electric changes associated with reptitive action in a non-medullated axon. *J. Physiol. (Lond.).* **116**:497–509.
20. HODGKIN, A. L., and A. F. Huxley. 1952. Currents carried by sodium and potassium ions through the membrane of the giant axon of *Loligo*. *J. Physiol. (Lond.).* **116**:449–472.
21. HODGKIN, A. L., and A. F. HUXLEY. 1952. The dual effect of membrane potential on sodium conductance in the giant axon of *Loligo*. *J. Physiol., (Lond.).* **116**:497–506.
22. HODGKIN, A. L., and A. F. HUXLEY. 1952. A quantitative description of membrane current and its application to conduction and excitation in nerve. *J. Physiol. (Lond.).* **117**:500–544.
23. HODGKIN, A. L., A. F. HUXLEY, and B. KATZ. 1952. Measurement of current voltage relations in the membrane of the giant axon of *Loligo*. *J. Physiol. (Lond.).* **116**:424–448.
24. HOYT, R. C., and W. J. ADELMAN. 1970. Sodium inactivation. Experimental test of two models. *Biophys. J.* **10**:610.
25. HUXLEY, A. F. 1959. Ion movements during nerve activity. Ann. N.Y. Acad. Sci. **81**:221–246.
26. JACK, J. J. B., D. NOBLE, and R. W. Y TSIEN. 1975. Electric current flow in excitable cells. Clarendon Press, Oxford University Press, London, U.K. 305–378.
27. KERNELL, D., and H. SJÖHOLM. 1973. Repetitive impulse firing; comparison between neurone models based on "Voltage clamp equations" and spinal motoneurones. *Acta Physiol. Scand.* **87**:40–56.
28. MOORE, J. W., and F. RAMON. 1974. On numerical integration of the Hodgkin and Huxley equations for a membrane action potential. *J. Theor. Biol.* **45**:249–273.
29. MOORE, J. W., and E. B. COX. 1976. A kinetic model for the sodium conductance system in squid axon. *Biophys. J.* **16**:171–192.
30. PARTRIDGE, L. D., and C. F. STEVENS. 1976. A mechanism for spike frequency adaptation. *J. Physiol. (Lond.).* **256**:315–332.
31. SHAPIRO, B. I., and F. K. LENHERR. 1972. Increased modulation and linearity to response to constant current stimulus. *Biophys. J.* **12**:1145–1158.

32. STEIN, R. B. 1967. The frequence of nerve action potentials generated by applied currents. *Proc. R. Soc. Lond. B. Biol. Sci.* **167**:64–86.
33. TOMITA, T., and E. B. WRIGHT. 1965. A study of the crustacean axon repetitive response. I. The effect of membrane potential and resistance. *J. Cell Comp. Physiol.* **65**:195–210.
34. VALLBO, A. B. 1964. Accomodation related to the inactivation of the sodium permeability in single myelinated nerve fibres from *Xenopus laevis*. *Acta Physiol. Scand.* **61**:429–444.
35. WRIGHT, E. B., and T. A. TOMITA. 1965. A study of the crustacean axon repetitive response. II. The effects of cation, sodium, calcium (magnesium), potassium and hydrogen (pH) in the external medium. *J. Cell Comp. Physiol.* **65**:211–228.

APPENDIX: DEFINITION OF PARAMETERS

The governing differential equation for the axon membrane is: $I(t) = C(dV/dT) + g_L(V\text{-}E_L) + g_{Na}(V\text{-}E_{Na}) + g_K(V\text{-}E_K) + g_A(V\text{-}E_K)$.

Sodium Conductance, g_{Na}

Sodium conductance has the usual definition: $\bar{g}_{Na} = g_{Na} m^3 h$. Squid axon data (22) were used as the basis for constructing the m and h functions used in the present computations. The data were modified as discussed earlier by shifting the voltage dependence of the parameters.

For m:

$$\alpha_m = \frac{-0.1(V_m + 35 + MSHFT)}{\exp\left\{\frac{-(V_m + 35 + MSHFT)}{10} - 1\right\}},$$

$\beta_m = 4\exp[-(V_m + 60 + MSHFT)/18]$. m_∞ and τ_m are defined for computation as $m_\infty = \alpha_m/(\alpha_m + \beta_m)$ and $\tau_m = (1/3.8)[1/(\alpha_m + \beta_m)]$, where $\tau_m(d_m/dt) + m = m_\infty$, and the number 3.8 is a temperature scaling factor. For h:

$$\alpha_h = 0.07\exp\left[\frac{-(V_m + 60 + HSHFT)}{20}\right]$$

and

$$\beta_h = \frac{1}{\exp\left[\frac{-(V_m + 30 + HSHFT)}{10} + 1\right]}.$$

Definitions for h_∞ and τ_h are analogous to those for m_∞ and τ_m.

The "m" parameters were moved 5.3 mV to the right on the voltage axis (MSHFT = −5.3) and the h parameters 12 mV to the right (HSHFT = −12). The m_∞ and h_∞ curves then intersected at 0.27. Shifting both parameters in this manner placed spike threshold at a value corresponding to microelectrode measurements (Connor, unpublished). E_{Na} retains its usual value, +55 mV and $\bar{g}_{Na} = 120$ mmho/cm^2.

Delayed Potassium Conductance, g_K

This parameter also has the usual definition: $g_K = \bar{g}_K n^4$. In constructing g_K the Hodgkin-Huxley data (22) were modified in the following ways: (*a*) $\bar{g}_K$ was reduced from 36 to 20

mmho/cm^2; (*b*) τ_n was multiplied by a factor of 2; (*c*) the n_∞ curve was shifted 4.3 mV to the right on the voltage axis. The usual value of E_K was used, −72 mV.

For n: $\alpha_n = -0.01(V_m + 50 + \text{NSHFT})/\{\exp[-(V_m + 50 + \text{NSHFT})/10] - 1\}$, $\beta_n = 0.125 \exp[-(V_m + 60 + \text{NSHFT})/80]$, NSHFT = −4.3 mV, $n_\infty = \alpha_n/(\alpha_n + \beta_n)$, and $\tau_n = (2/3.8)[1/(\alpha_n + \beta_n)]$.

Transient Potassium Conductance, g_A

$g_A = \bar{g}_A A^3 B$. The functions A_∞, τ_A, B_∞, and τ_B are given graphically in Fig. 3. The standard value of $\bar{g}_A$ is 47.7 but several series of computations have been made with $\bar{g}_A$ reduced to 33. The A and B factors have the same functional significance as the m and h factors of the sodium conductance system. That is: $\tau_A(dA/dt) + A = A_\infty$, and $\tau_B(dB/dt) + B = B_\infty$. The equilibrium battery for the transient potassium conductance was made slightly more negative than E_K, $E_A = -75$ mV. Analytic expressions for I_A parameters used in computation are:

$$A_\infty = \left[0.0761 \frac{\exp[(V_m + 94.22)/31.84]}{1 + \exp[(V_m + 1.17)/28.93]}\right]^{1/3},$$

$$\tau_A = 0.3632 + \frac{1.158}{1 + \exp[(V_m + 55.96)/20.12]},$$

$$B_\infty = \frac{1}{\{1 + \exp[(V_m + 53.3)/14.54]\}^4},$$

and

$$\tau_B = 1.24 + \frac{2.678}{1 + \exp[(V_m + 50)/16.027]}$$

Capacitance and Leakage Conductance, C_M and g_L

Squid axon values were used, *i.e.* $C_M = 1\ \mu\text{F/cm}^2$ and $g_L = 0.3$ mmho/cm^2. In most calculations it was necessary to alter the value of E_L from the usual value to −17 mV to counterbalance certain effects of I_A. The values delineated in this section will be defined as standard parameters.